Adaptive Robust Motion Control for Hydraulic Actuators With an Adjustable Event Trigger

Jixiang Chen, Zhongyang Fei, *Senior Member, IEEE*, Litong Lyu, Weiguo Xia, *Member, IEEE*, and Xi-Ming Sun, *Senior Member, IEEE*

***Abstract*—This article investigates the event-triggered adaptive robust motion control for hydraulic actuators with parametric uncertainties and system nonlinearities. Under the continuous communication condition, the traditional adaptive robust motion controller is recursively presented. In order to reduce the unnecessary bandwidth consumption in the aero-engine networked control platform, an adaptive threshold triggered mechanism according to network resources is developed to synthesize the motion controller. Adjustable threshold parameters are involved to flexibly adjust the data transmission times depending on the network bandwidth occupation. It is proved that with the motion controller and the proposed adjustable threshold triggered mechanism, all the closed-loop system signals are globally bounded, and the hydraulic system output achieves asymptotic tracking to the reference trajectory by virtue of the adaptive technique, the Nussbaum-type and sign functions. Besides, the Zeno behavior is excluded, successfully. Finally, the proposed event-based control scheme is tested and discussed on the aero-engine hardware-in-the-loop (HIL) experiment platform with hydraulic actuators.**

***Index Terms*—Adaptive robust control (ARC), adjustable threshold triggered mechanism, hydraulic actuators, motion control.**

I. Introduction

HYDRAULIC actuators have been widely applied in industry due to their advantages of small size-to-power ratio and large force/torque output capability [1], [2], [3], [4], [5]. Actually, to achieve better motion control performance, the model-based control strategies are frequently used for the design of accurate motion controllers, such as adaptive backstepping technique [6], feedback linearization technique [7], and high-gain control technique [8]. In recent years, by virtue of the rapid development of the network communication technique, the networked control systems are broadly implemented in many applications since this configuration brings great convenience to multiobjective information transformation, coordination of different tasks and more compact industrial site space [9]. Unavoidably, when the hydraulic sensors, actuators, and controllers are located at the networked control systems, these model-based control schemes require that the system states and measured outputs are sampled in a fixed interval, which is also called the time-triggered or periodic sampling control. Although such sampling control algorithm facilitates to synthesize and analyze the hydraulic system, lots of network resources are consumed and wasted in the case that no obvious state changes [10], [11], [12], [13], [14], [15]. As the communication resource is generally restricted, especially for the networked control systems [16], it has become an important problem on how to reduce the conservatism or limitation for the motion control schemes in terms of the bandwidth occupation.

To save the valuable network resource, event-based control strategies have been extensively studied [9], [10], [11], [12], [16], [17], [18], [19], [20], [21]. The event-triggered control concept was proposed in [9], and numerous event-triggered control schemes were designed by input-to-state stable (ISS) assumption. Recently, the event-triggered strategies were introduced to model-based control [18], [19], [20]. It is easy to check that the ISS assumption is hard to be fulfilled in the presence of uncertainties. Fortunately, a great improvement of removing the ISS assumption was acquired in [19] which designed the event-based control schemes with a new co-design idea. However, it is worth noting that these event triggers used in the aforementioned literature neglect the influence of bandwidth occupation, such as the busy communicating mode and the idle mode. In the congesting mode, the mentioned static triggering mechanisms may be conservative in terms of bandwidth-saving. Instead, when the communication network is idle, the predefined triggering strategies work with a small amount of triggering times, which is possibly not conducive to raising the bandwidth utilization. In addition, the model-based event-triggered control schemes only achieved the bounded results. Clearly, they generate some limitations to obtain better output tracking or the asymptotic tracking

Received 10 September 2024; revised 7 February 2025; accepted 9 June 2025. Date of publication 15 July 2025; date of current version 18 September 2025. This work was supported in part by the Bolian Research Funds of Dalian Maritime University and the Fundamental Research Funds for the Central Universities under Grant 3132025601; in part by the National Natural Science Foundation of China under Grant 62273069; in part by the National Natural Science Foundation of Liaoning Province under Grant 2024-MSBA-02; and in part by the Science and Technology Project of Hebei Education Department under Grant BJ2025200 Youth Talent Program Supported by China Railway Society. This article was recommended by Associate Editor L. Sheremetov. *(Corresponding author: Zhongyang Fei.)*

Jixiang Chen is with the College of Marine Electrical Engineering, Dalian Maritime University, Dalian 116026, China (e-mail: chenjixiang@dlmu.edu.cn).

Zhongyang Fei, Weiguo Xia, and Xi-Ming Sun are with the Key Laboratory of Intelligent Control and Optimization for Industrial Equipment of Ministry of Education, Dalian University of Technology, Dalian 116024, China (e-mail: zhongyangfei@dlut.edu.cn; wgxiaseu@dlut.edu.cn; sunxm@dlut.edu.cn).

Litong Lyu is with the School of Mechanical Engineering, Shijiazhuang Tiedao University, Shijiazhuang 050043, China (e-mail: litong_lyu@stdu.edu.cn).

Color versions of one or more figures in this article are available at https://doi.org/10.1109/TSMC.2025.3581240.

Digital Object Identifier 10.1109/TSMC.2025.3581240

performance for hydraulic system, compared to the traditional methods, such as in [2], [22], and [23]. To overcome the main limitation of mere boundedness, the authors in [11] and [24] proposed some event-based control strategies to ensure the zero stabilization error. Nevertheless, the primary motion control objective of hydraulic actuators is to accurately track the reference trajectory, which cannot be directly performed using the methods from [11] and [24].

For electro-hydraulic actuators, it should be pointed out that there is an assortment of intractable problems within motion control, such as parametric uncertainties and uncertain nonlinearities [6]. In fact, the adaptive estimation technique has proven to be an effective technique to handle the complex unknowns for various uncertain nonlinear systems [24], [25], [26]. As a result, the adaptive technique was early applied to solve parametric uncertainties for the hydraulic system [2]. Furthermore, the works in [2] introduced the deterministic robust control to synthesize the adaptive robust controller (ARC), thereby contributing to better guaranteed transient performance than the adaptive control alone in the presence of system nonlinearities. Since then, ARC and its modifications have been applied to many practical physical systems, e.g., the valve and pump combined systems [22], the linear motors [27], the robot manipulators [28], and vehicle suspensions [29].

Inspired by the above discussion, it would be exciting if the asymptotic output tracking with limited communication resources can be ensured and the network communications with heavy bandwidth occupation can be alleviated, simultaneously. To be specific, the ARC technique is adopted and presented as the virtual controller of the event-based control scheme. A novel adjustable threshold triggered mechanism is then proposed to synthesize the event-based ARC controller, but without the Zeno behavior. The main contributions of this study can be illustrated as below.

1) The measurement error, caused by the event-triggered rule, is resolved by the Nussbaum function, instead of $\tanh(\cdot)$ used in most references, such as [19] and [30]. Therefore, the robustness of the closed-loop system can be further improved by virtue of the designed dynamic updating law compared to the fixed gain used in $\tanh(\cdot)$.
2) The asymptotic output tracking performance is achieved with the proposed control strategy, rather than the merely bounded results in [10], [19], and [20].
3) The proposed event-triggered mechanism can reduce the amount of data sent in the congesting communication mode, and also increase the transmission times in the idle mode, thus improving the tracking precision.

The bus-topology protocol, due to its simple structure, convenient operation, and easy maintenance, is always utilized for the network transmission channels among modern industrial devices. The aero-engine networked control platform, as one typical scenario of many similar applications, is used to test and verify the proposed event-based motion control scheme, as plotted in Fig. 1. The value of the control voltage is sent to the servo-valve through these network transmission channels based on the adjustable event trigger. In the meantime, the state information is periodically sampled and transferred to the networked controller with the same network

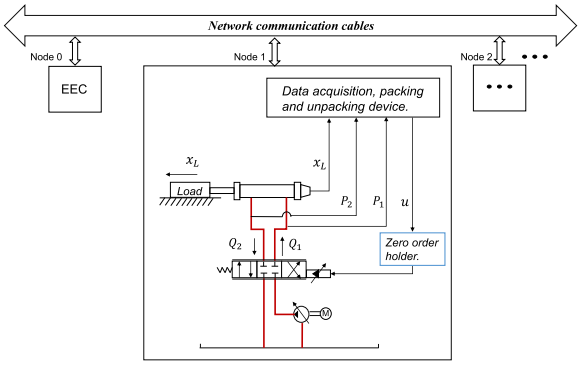

Fig. 1. Aero-engine HIL experiment platform.

transmission channels. Furthermore, this platform select an electronic engine controller (EEC) as the networked controller that can be invoked to execute the proposed control algorithm. Experimental results will be displayed to show the high performance for the limited bandwidth by contrast to the traditional ARC schemes [2], as well as the flexibility of the presented adaptive event-triggered mechanism, compared to the static mechanisms, as presented in [11], [19], and [20].

The remainder of this article is organized as follows. Section II formulates the problem and constructs the system model. Section III proposes the adaptive threshold triggered mechanism and designs the event-triggered ARC motion controller. Section IV discusses the results of the experiment. Finally, the proposed scheme is concluded in Section V.

II. System Modeling and Problem Formulation

This article considers the single-rod hydraulic cylinder system in the aero-engine hardware-in-the-loop (HIL) platform which has the similar form as in [2]. The inertia load dynamics can be modeled as

$$M\ddot{x}_L = F_L - B_f\dot{x}_L - A_f\mathcal{S}(\dot{x}_L) + F \tag{1}$$

where $F_L = A_1P_1 - A_2P_2$ is the load force, $\dot{x}_L$ and $\ddot{x}_L$ are velocity and acceleration of the load, B_f and A_f denote some coefficients, and F is the lumped force uncertainty. All symbol definitions can be found in the notation list. Here, $\mathcal{S}(\dot{x}_L)$ denotes a known smooth function that is used to approximate the discontinuous sign function, like $(2/\pi)\text{atan}(1000\bullet)$ in [22].

The hydraulic cylinder dynamics is expressed as

$$V_{h1}(x_L)\beta_e^{-1}\dot{P}_1 = -A_1\dot{x}_L + Q_1 + D_1 \tag{2}$$

$$V_{h2}(x_L)\beta_e^{-1}\dot{P}_2 = +A_2\dot{x}_L - Q_2 - D_2 \tag{3}$$

where $V_{h1}(x_L) = V_{01}+A_1x_L$, $V_{h2}(x_L) = V_{02}-A_2x_L$, D_1 and D_2 represent the flow rate uncertainties. For simplification, these symbols are also explained in the notation list. The hydraulic cylinder flow rates Q_1 and Q_2 can be given as [1]

$$Q_1 = k_{q1}x_\upsilon\left(\mathbf{s}(x_\upsilon)\sqrt{P_s - P_1} + \mathbf{s}(-x_\upsilon)\sqrt{P_1 - P_r}\right) \tag{4}$$

$$Q_2 = k_{q2}x_\upsilon\left(\mathbf{s}(x_\upsilon)\sqrt{P_2 - P_r} + \mathbf{s}(-x_\upsilon)\sqrt{P_s - P_2}\right) \tag{5}$$

where x_υ is the spool displacement from neutral, the symbol $\mathbf{s}(\star) = 1\ \forall\star \geq 0$ or $\mathbf{s}(\star) = 0\ \forall\star < 0$ and flow coefficients $k_{q1} = C_da_1\sqrt{2/\rho}, k_{q2} = C_da_2\sqrt{2/\rho}$ in which C_d is the

discharge coefficient, a_1, a_2 represent the area gradient, and ρ denotes the oil density. Actually, the servo valve dynamics is omitted in the experiments due to faster servo valve response compared to practical work frequency range of the cylinder. Hence, it can be assumed that the displacement x_v is directly proportional to the input voltage signal u, i.e., $x_v = k_v u$, where k_v is a positive electrical constant [22]. Define the following symbols for simplification:

$$\begin{cases} s_1 = A_1/V_{h1}(x_L),\ s_2 = A_2/V_{h2}(x_L) \\ f \triangleq f(x_L, \dot{x}_L) = (s_1 A_1 + s_2 A_2)\dot{x}_L \\ g \triangleq g(x_L, P_1, P_2, u) = s_1 k_v k_{q1} g_1 + s_2 k_v k_{q2} g_2 \\ g_1 = \mathbf{s}(u)\sqrt{P_s - P_1} + \mathbf{s}(-u)\sqrt{P_1 - P_r} \\ g_2 = \mathbf{s}(u)\sqrt{P_2 - P_r} + \mathbf{s}(-u)\sqrt{P_s - P_2}. \end{cases} \tag{6}$$

Introduce the state variables $[x_1, x_2, x_3] = [x_L, \dot{x}_L, F_L]$ and arrange the hydraulic system in the state space form

$$\begin{aligned} \dot{x}_1 &= x_2 \\ \dot{x}_2 &= \frac{1}{M}\left(x_3 - B_f x_2 - A_f \mathcal{S}(x_2)\right) + F_M \\ \dot{x}_3 &= \beta_e g u - \beta_e f + s_1 D_{1\beta} + s_2 D_{2\beta} \end{aligned} \tag{7}$$

where $F_M = F/M$, $D_{1\beta} = D_1\beta_e$, and $D_{2\beta} = D_2\beta_e$.

Assumption 1: The desired trajectory $x_d(t)$ and its first 3-rd order derivatives are piecewise continuous, known, and bounded.

Given the desired motion trajectory $x_d(t)$, our *control objective* is to synthesize the event-triggered control law u such that the system output x_L tracks the signal $x_d(t)$ as closely as possible with parametric uncertainties and uncertain nonlinearities. Meanwhile, the event-triggered mechanism should reduce the network communication burden of congesting mode, and make full use of idle network resources.

III. Event-Triggered ARC Design

The present section first derives the continuous communication-based ARC motion controller [2]. Meanwhile, we develop the event-triggered mechanism and synthesize the event-driven ARC motion control scheme.

The controller structure is displayed in Fig. 2. Note that the time-triggered ARC controller ensures the intermediate signals α_{3a}, α_{3s}, which are treated as virtual control inputs of the event-triggered control. Based on the design parameters σ, m and the adaptive threshold ϵ_j, the time-based sampling control input $\mu(t)$ is obtained, and the control signal is sent to hydraulic system according to the proposed event trigger.

A. Design Model and Discontinuous Projection Mapping

To handle the parametric uncertainties, an unknown parameter set is defined as $\theta^T = [\theta_1, \theta_2, \theta_3, \theta_4, \theta_5, \theta_6, \theta_7] = [1/M, B_f/M, A_f/M, \bar{F}_M, \beta_e, \bar{D}_{1\beta}, \bar{D}_{2\beta}]$. Note from (7) that

$$\begin{aligned} \dot{x}_1 &= x_2 \\ \dot{x}_2 &= \theta_1 x_3 - \theta_2 x_2 - \theta_3 \mathcal{S}(x_2) + \theta_4 + \Delta_1 \\ \dot{x}_3 &= \theta_5 g u - \theta_5 f + s_1\theta_6 + s_2\theta_7 + \Delta_2 \end{aligned} \tag{8}$$

where $\Delta_1 = F_M - \bar{F}_M$, $\Delta_2 = s_1\tilde{D}_{1\beta} + s_2\tilde{D}_{2\beta}$, $\tilde{D}_{1\beta} = D_{1\beta} - \bar{D}_{1\beta}$, $\tilde{D}_{2\beta} = D_{2\beta} - \bar{D}_{2\beta}$. In general, $\bar{F}_M, \bar{D}_{1\beta}, \bar{D}_{2\beta}$ represent, respectively, the nominal or low-frequency values of lumped disturbance force F_M and flow rates $D_{1\beta}, D_{2\beta}$. In parallel, the nonlinearities Δ_1 and Δ_2 represent these components that are difficult to estimate.

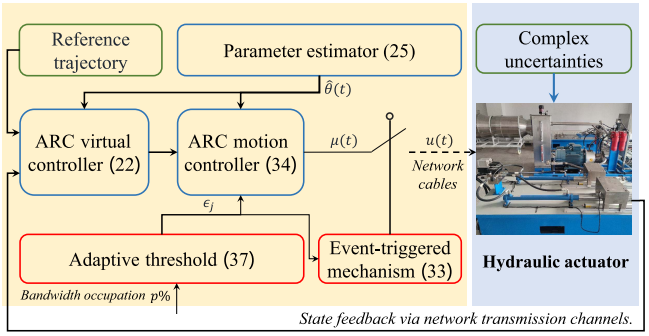

Fig. 2. Structure of the presented event-based ARC motion controller.

In the practical hydraulic system, the unknown physical parameters and uncertain nonlinearities are always assumed to be bounded, as in [2].

Assumption 2: The unknown parameters and nonlinearities of the hydraulic system are in known compact sets such that

$$\begin{aligned} \theta \in \Omega_\theta &\triangleq \left\{\theta_{p\min} \le \theta_p \le \theta_{p\max}, p = 1, 2, \ldots, 7\right\} \\ \Delta_i \in \Omega_\Delta &\triangleq \{\Delta_i : |\Delta_i| < \delta_i(t), i = 1, 2\} \end{aligned}$$

where $\theta_{p\min}, \theta_{p\max}$, and $\delta_i(t)$ are known boundaries [2].

To estimate these uncertain parameters, this article utilizes the projection mapping adaptive law from [2]. Let $\hat{\star}$ be the estimate of the unknown constant $\star$ and $\tilde{\star}$ be the parameter estimation error (i.e., $\tilde{\star} = \hat{\star} - \star$). It can be then given by

$$\mathrm{Proj}_{\hat{\theta}_i}(\star_i) = \begin{cases} 0, & \text{if } \hat{\theta}_i = \theta_{iM} \text{ and } \star_i > 0 \\ 0, & \text{if } \hat{\theta}_i = \theta_{im} \text{ and } \star_i < 0 \\ \star_i, & \text{otherwise} \end{cases}$$

where $i = 1, 2, \ldots, 7$. Denote $\tau(t) \in \mathbb{R}^7$ as any continuous function and $\Gamma \in \mathbb{R}^{7\times 7}$ as a positive define diagonal matrix, and $\Gamma = \mathrm{diag}\{\gamma_1, \gamma_2, \ldots, \gamma_7\}$, where $\gamma_1, \gamma_2, \ldots, \gamma_7$ are the tunable gains. If we choose the adaptive law as follows:

$$\dot{\hat{\theta}} = \mathrm{Proj}_{\hat{\theta}}(\Gamma\tau(t)), \theta_{\min} \le \hat{\theta}(0) \ \le \theta_{\max} \tag{9}$$

there are double advantages as mentioned in [22]

$$\begin{cases} (P1): \hat{\theta} \in \Omega_\theta = \{\hat{\theta}{:}\theta_{\mathrm{m}} \le \hat{\theta} \le \theta_M\} \\ (P2): \tilde{\theta}^T\left(\Gamma^{-1}\mathrm{Proj}_{\hat{\theta}}(\Gamma\tau(t)) - \tau(t)\right) \le 0. \end{cases} \tag{10}$$

B. ARC Virtual Motion Controller

This section derives the standard ARC motion controller for a single-rod hydraulic actuator [2], [22]. Traditional ARC motion controller can be treated as a virtual motion control law of the event-based control scheme.

Step 1: Due to no uncertainties included in the first equation of (8), a virtual control law can be constructed for the first two equations. Define the switching-function-like variable as

$$z_2 = \dot{z}_1 + k_1 z_1 = x_2 - \dot{r}, \quad \dot{r} \triangleq -k_1 z_1 + \dot{x}_d \tag{11}$$

where $z_1 = x_1 - x_d$ is the tracking error and $k_1 > 0$ denotes any feedback gain. By noting the transfer function $G_1(s) = (z_1(s)/z_2(s)) = 1/(s + k_1)$, if the error $z_2(t)$ converges to a

small set or zero, then the signal $z_1(t)$ converges to a small set or zero. Clearly, the control objective for tracking error $z_1(t)$ is transferred to the virtual error $z_2(t)$. Calculate the derivative of z_2 along the system (8) as

$$\dot{z}_2 = \theta_1 x_3 - \theta_2 x_2 - \theta_3 \mathcal{S}(x_2) + \theta_4 + \Delta_1 - \ddot{r}. \tag{12}$$

Denote $z_3 = x_3 - \alpha_2$ as virtual error and α_2 as the virtual control law, which can be chosen by

$$\begin{aligned} \alpha_2 &= \alpha_{2a} + \alpha_{2s} \\ \alpha_{2a} &= \frac{\hat{\theta}_2 x_2 + \hat{\theta}_3 \mathcal{S}(x_2) - \hat{\theta}_4 + \ddot{r}}{\hat{\theta}_1}, \alpha_{2s} = \alpha_{2s1} + \alpha_{2s2} \\ \alpha_{2s1} &= -\frac{1}{\theta_{1\min}} k_{2s} z_2, k_{2s} \geq k_2 + d_1 \frac{w_3}{w_2} \|\Gamma \phi_2 w_2\|^2 \end{aligned} \tag{13}$$

where $k_2 > 0$ is the feedback gain, w_2, w_3 denote the scaling factors, d_1 and α_{2s2} are the positive gain and the robust control law which are designed latter. The tuning function $\tau_2(t)$ is

$$\tau_2(t) = w_2 \phi_2 z_2 \tag{14}$$

where the regression vector ϕ_2 is defined as

$$\phi_2 = [\alpha_{2a}, -x_2, -\mathcal{S}(x_2), 1, 0, 0, 0]^T. \tag{15}$$

The nonlinear robust term α_{2s2} satisfies two conditions [2]

$$\begin{cases} (P1): z_2\left(\theta_1 \alpha_{2s2} - \tilde{\theta}^T \phi_2 + \Delta_1\right) \leq \varepsilon_1 \\ (P2): z_2 \theta_1 \alpha_{2s2} \leq 0 \end{cases} \tag{16}$$

where $\varepsilon_1 > 0$ is a design parameter which can be arbitrary small and $\tilde{\theta}^T = [\tilde{\theta}_1, \tilde{\theta}_2, \ldots, \tilde{\theta}_7]$. Inspired by [2] and [22], the robust control function α_{2s2} can be chosen as

$$\alpha_{2s2} = -\frac{h_1^2}{4\varepsilon_1} z_2 \tag{17}$$

where $h_1 \geq \|\phi_2^T(\theta_{\max} - \theta_{\min})\| + \delta_1$.

Applying the virtual input α_2 to the derivative of z_2 yields

$$\dot{z}_2 = \theta_1 z_3 - k_{2s} \frac{\theta_1}{\theta_{1\min}} z_2 + \theta_1 \alpha_{2s2} - \tilde{\theta}^T \phi_2 + \Delta_1. \tag{18}$$

Define $V_1 = (1/2) w_2 z_2^2$ and calculate the derivative along $\dot{z}_2$ as

$$\begin{aligned} \dot{V}_1 = {} & \theta_1 w_2 z_2 z_3 - w_2 k_{2s} \frac{\theta_1}{\theta_{1\min}} z_2^2 \\ & + w_2 z_2 \left(\theta_1 \alpha_{2s2} - \tilde{\theta}^T \phi_2 + \Delta_1\right) \end{aligned} \tag{19}$$

where $w_2 > 0$ is a design scaling factor.

Step 2: Equation (19) means that the system realizes control objectives when $z_3 = 0$ and (16) is also satisfied with the standard ARC arguments in [2]. Thus, this step synthesizes the virtual motion controller α_3 to make the virtual error z_3 small or converge to zero.

Calculate the derivative of the virtual error z_3 as

$$\begin{aligned} \dot{z}_3 &= \dot{x}_3 - \dot{\alpha}_2 \\ &= \theta_5 g u - \theta_5 f + s_1 \theta_6 + s_2 \theta_7 + \Delta_2 - (\dot{\alpha}_{2u} + \dot{\alpha}_{2c}) \end{aligned} \tag{20}$$

where $\dot{\alpha}_{2c}, \dot{\alpha}_{2u}$ are the calculable and incalculable parts of $\dot{\alpha}_2$ with the formulation listed as

$$\begin{aligned} \dot{\alpha}_2 &= \dot{\alpha}_{2c} + \dot{\alpha}_{2u}, \dot{\alpha}_{2c} = \frac{\partial \alpha_2}{\partial x_1} x_2 + \frac{\partial \alpha_2}{\partial x_2} \hat{\dot{x}}_2 + \frac{\partial \alpha_2}{\partial t} \\ \hat{\dot{x}}_2 &= \hat{\theta}_1 x_3 - \hat{\theta}_2 x_2 - \hat{\theta}_3 S(x_2) + \hat{\theta}_4 \\ \dot{\alpha}_{2u} &= \frac{\partial \alpha_2}{\partial \hat{\theta}} \dot{\hat{\theta}} + \frac{\partial \alpha_2}{\partial x_2} \left(\dot{x}_2 - \hat{\dot{x}}_2\right) = \frac{\partial \alpha_2}{\partial \hat{\theta}} \dot{\hat{\theta}} + \frac{\partial \alpha_2}{\partial x_2} \cdot \\ & \quad \left(-\tilde{\theta}_1 x_3 + \tilde{\theta}_2 x_2 + \tilde{\theta}_3 S(x_2) - \tilde{\theta}_4 + \Delta_1\right) \end{aligned} \tag{21}$$

where $\hat{\dot{x}}$ stands for the estimate of $\dot{x}_2$.

The virtual motion controller α_3 is designed as

$$\begin{aligned} \alpha_3 &= \alpha_{3a} + \alpha_{3s} \\ \alpha_{3a} &= \frac{1}{g\hat{\theta}_5} \left(-s_1 \hat{\theta}_6 - s_2 \hat{\theta}_7 + \dot{\alpha}_{2c} + \hat{\theta}_5 f - \frac{w_2}{w_3} \hat{\theta}_1 z_2\right) \\ \alpha_{3s} &= \alpha_{3s1} + \alpha_{3s2}, \alpha_{3s1} = -\frac{1}{g\theta_{5\min}} k_{3s} z_3 \\ k_{3s} &\geq k_3 + d_1 \|\Gamma \phi_3 w_3\|^2 + d \left\| \frac{\partial \alpha_2}{\partial \hat{\theta}} \right\|^2 \end{aligned} \tag{22}$$

where k_3 is any positive feedback gain, d and α_{3s2} are the design constants and the robust control law, which are given latter. Moreover, the adaptive function $\tau_3(t)$ is given by

$$\tau_3(t) = w_2 \phi_2 z_2 + w_3 \phi_3 z_3 \tag{23}$$

where the regression vector function ϕ_3 refers to

$$\begin{aligned} \phi_3^T = \Bigg[& \frac{w_2}{w_3} z_3 - \frac{\partial \alpha_2}{\partial x_2} x_3, \ \frac{\partial \alpha_2}{\partial x_2} x_2 \\ & \frac{\partial \alpha_2}{\partial x_2} S(x_2), \ -\frac{\partial \alpha_2}{\partial x_2}, \ g\alpha_{3a} - f, \ s_1, \ s_2 \Bigg]. \end{aligned} \tag{24}$$

Therefore, the adaptive law is designed as

$$\dot{\hat{\theta}}(t) = \mathrm{Proj}_{\hat{\theta}}(\Gamma \tau_3(t)). \tag{25}$$

From (21), it is easy to check that the incalculable part $\dot{\alpha}_{2u}$ is suppressed by the nonlinear robust control law. Hence, the nonlinear feedback term α_{3s2} is chosen to satisfy conditions

$$\begin{cases} (P1): z_3 \left(\theta_5 g \alpha_{3s2} - \tilde{\theta}^T \phi_3 + \Delta_2 - \frac{\partial \alpha_2}{\partial x_2} \Delta_1\right) \leq \varepsilon_2 \\ (P2): z_3 g \theta_5 \alpha_{3s2} \leq 0 \end{cases} \tag{26}$$

where $\varepsilon_2 > 0$ is an arbitrarily small design constant. Then, α_{3s2} is designed as the following form:

$$\alpha_{3s2} = -\frac{h_2^2(x)}{g\theta_{5\min} 4\varepsilon_2} z_3 \tag{27}$$

where $h_2 \geq \|\theta_{\max} - \theta_{\min}\| \|\phi_3(x)\| + |(\partial \alpha_2 / \partial x_2)| \delta_1 + \delta_2$. Together with (20) and (22), we have the fact

$$\begin{aligned} \dot{z}_3 = {} & \theta_5 g e_u - \frac{w_2}{w_3} \theta_1 z_2 - k_{3s} \frac{\theta_5}{\theta_{5\min}} z_3 - \frac{\partial \alpha_2}{\partial \hat{\theta}} \dot{\hat{\theta}} \\ & + \theta_5 \alpha_{3s2} - \tilde{\theta}^T \phi_3 + \Delta_2 - \frac{\partial \alpha_2}{\partial x_2} \Delta_1 \end{aligned} \tag{28}$$

where $e_u = u - \alpha_3$. Choose the Lyapunov function $V_2 = V_1 + (1/2) w_3 z_3^2$ and derive it along (28) yielding

$$\begin{aligned} \dot{V}_2 = \dot{V}_1 + w_3 z_3 \Bigg[& \theta_5 g e_u - \frac{w_2}{w_3} \theta_1 z_2 - k_{3s} \frac{\theta_5}{\theta_{5\min}} z_3 \\ & + \theta_5 g \alpha_{3s2} - \tilde{\theta}^T \phi_3 + \Delta_2 - \frac{\partial \alpha_2}{\partial x_2} \Delta_1 - \frac{\partial \alpha_2}{\partial \hat{\theta}} \dot{\hat{\theta}} \Bigg] \end{aligned} \tag{29}$$

where $w_3 > 0$. Using Young's inequality obtains

$$z_3\frac{\partial\alpha_2}{\partial\hat{\theta}}\dot{\hat{\theta}} \le d\left\|\frac{\partial\alpha_2}{\partial\hat{\theta}}\right\|^2 z_3^2 + d_1\|\Gamma\phi_2\|^2 w_2^2 z_2^2 + d_1\|\Gamma\phi_3\|^2 w_3^2 z_3^2 \quad (30)$$

where $d > 0$ is a constant, d_1 satisfies $d_1 > 1/(2d)$, and

$$\|\dot{\hat{\theta}}\|^2 = \|\mathrm{Proj}(\Gamma\tau_3)\|^2 \le \|\Gamma(w_2\phi_2 z_2 + w_3\phi_3 z_3)\|^2 \le 2\Big(\|\Gamma\phi_2\|^2 w_2^2 z_2^2 + \|\Gamma\phi_3\|^2 w_3^2 z_3^2\Big). \quad (31)$$

In the end, substituting (30) and (31) into (29) has

$$\dot{V}_2 \le -w_2 k_2 z_2^2 - w_3 k_3 z_3^2 + w_2\varepsilon_1 + w_3\varepsilon_2 + w_3 z_3\theta_5 g e_u. \quad (32)$$

C. Event-Triggered ARC Motion Controller

In this section, the adaptive threshold triggered mechanism is proposed and applied to co-design the event-triggered ARC motion controller for hydraulic actuators.

It is supposed that the system control signal is sampled and transmitted via the network transmission channel at time sequence $\{t_j, j \in \mathbb{Z}\}$ satisfying $0 = t_0 < t_1 < \cdots < t_j < \cdots$ Now, we directly give the adaptive threshold triggered mechanism as follows:

$$t_{j+1} = \big\{t > t_j \big| |e(t)| > \sigma_j|u(t)| + m_j\big\} \quad (33)$$

where $e(t) = u(t) - \mu(t)$ is the measurement error, $\mu(t)$ represents the time-based sampling control law, which is

$$\mu(t) = -N(\xi)\alpha_{3a} + \big(1+\sigma_j\big)\alpha_{3s} - \mathrm{sign}(z_3)m_j \quad (34)$$

where $\sigma_j = \epsilon_j\sigma, m_j = \epsilon_j m$, and $0 < \sigma < 1$, $m > 0$ are the design parameters, the function $N(\xi) = \xi^2\cos(\xi)$ is the Nussbaum-type function [31], $\xi(t)$ is the solution to the differential equation

$$\dot{\xi}(t) = -g\alpha_{3a}z_3. \quad (35)$$

Here, $\mathrm{sign}(\cdot)$ represents the sign function [11] and $\epsilon_j \in [0.1, 1]$ is a monotone nondecreasing function of the current network bandwidth occupation $p\%$.

Eventually, define the event-triggered ARC control law as

$$u(t) = \mu\big(t_j\big)\ \forall t \in \big[t_j, t_{j+1}\big). \quad (36)$$

Remark 1: Clearly, under the premise of assuring the control performance, the proposed triggered mechanism (33) changes the amount of triggered times following the parameters σ_j, m_j. After introducing the adjustable threshold ϵ_j, the parameters σ_j, m_j turn to be adjustable. On one hand, (33) can generate less amount of triggered times by increasing the value of threshold ϵ_j, which reduces the communication burden of the heavy network bandwidth occupation. On the other hand, (33) raises the utilization of network resources when the network bandwidth is idle, with a smaller value of threshold ϵ_j, thereby achieving more high tracking precision. As in [18], a simple form of the function ϵ_j can be given by

$$\epsilon_j = \begin{cases} p/100, & p \in [10, 100] \\ 0.1, & \text{otherwise} \end{cases} \quad (37)$$

where $p\%$ represents the network bandwidth occupation.

Remark 2: There are mainly two merits on using $N(\xi)$ in this article, instead of $\tanh(\cdot)$ used in previous results, e.g., [19], [30]. First, $N(\xi)$ is easily utilized with the updating law $\dot{\xi}(t)$, but $\tanh(\cdot)$ requires to predefine a fixed gain. Thus, $N(\xi)$ can improve the system robustness in terms of selecting gains. Second, $N(\xi)$ enables to achieve the asymptotic tracking performance. Instead, the nonlinear control using $\tanh(\cdot)$ only holds the bounded results.

D. Stability Analysis and Avoidance of Zeno Phenomenon

The present section establishes the stability, and avoids the Zeno behavior with respect to the closed-loop hydraulic system under the proposed event-based ARC law. These results are collected in Theorem 1.

Theorem 1: Consider the hydraulic system (8) with control law (36), adaptive threshold triggered mechanism (33), and the adaptive law (25). If Assumptions 1 and 2 are satisfied, all signals of the closed-loop system are bounded by

$$V_2(t) \le V_2(0)e^{-k_0 t} + \frac{\varepsilon}{k_0}\Big(1 - e^{-k_0 t}\Big) + \varpi \quad (38)$$

where $k_0 = \min\{2k_2, 2k_3\}$, $\varepsilon = w_2\varepsilon_1 + w_3\varepsilon_2$ and ϖ is a known bounded constant. Further, if, after a finite time, $\Delta_1 = \Delta_2 = 0$, i.e., the hydraulic system is only with parametric uncertainties, the hydraulic system performs asymptotic output tracking, i.e., $z_1(t) \to 0$ as $t \to \infty$. Besides, there is a scalar $T > 0$ such that $t_{j+1} - t_j \ge T\ \forall j = 0, 1, 2, \ldots,$ hold.

Proof: As in [19], the control law (36) is derived by

$$u(t) = \frac{1}{1-\lambda_1(t)\sigma_j}\mu(t) + \frac{\lambda_2(t)}{1-\lambda_1(t)\sigma_j}m_j \quad (39)$$

where $-1 \le \lambda_1(t) \le 1$ and $-1 \le \lambda_2(t) \le 1$.

Applying (39) to (32), we get

$$\dot{V}_2 = -w_2k_2z_2^2 - w_3k_3z_3^2 + w_2\varepsilon_1 + w_3\varepsilon_2 + w_3\theta_5 g\left(\frac{-N(\xi)z_3\alpha_{3a}}{1-\lambda_1(t)\sigma_j} - z_3\alpha_{3a}\right) \quad (40a)$$

$$+ w_3\theta_5 g\left(\frac{(1+\sigma_j)z_3\alpha_{3s}}{1-\lambda_1(t)\sigma_j} - z_3\alpha_{3s}\right) \quad (40b)$$

$$+ w_3\theta_5 g\left(\frac{-|z_3|m_j - z_3\lambda_2(t)m_j}{1-\lambda_1(t)\sigma_j}\right). \quad (40c)$$

Note that (40a) is first calculated as

$$w_3\theta_5 g\left(\frac{-N(\xi)z_3\alpha_{3a}}{1-\lambda_1(t)\sigma_j} - z_3\alpha_{3a}\right) = w_3\theta_5(\nu(t)N(\xi) + 1)\dot{\xi} \quad (41)$$

where $\nu(t) = 1/((1-\lambda_1(t)\sigma_j))$. We derive (40b) with the aid of $z_3\alpha_{3s} \le 0$ as

$$w_3\theta_5 g\left(\frac{(1+\sigma_j)z_3\alpha_{3s}}{1-\lambda_1(t)\sigma_j} - z_3\alpha_{3s}\right) \le w_3\theta_5 g\left(\frac{(1+\sigma_j)z_3\alpha_{3s}}{1+\sigma_j} - z_3\alpha_{3s}\right) = 0. \quad (42)$$

The term (40c) can be rewritten as

$$w_3\theta_5 g\left(\frac{-|z_3|m_j - z_3\lambda_2(t)m_j}{1-\lambda_1(t)\sigma_j}\right)$$

$$\leq w_3\theta_5 g\left(\frac{-|z_3|m_j+|z_3|m_j}{1-\lambda_1(t)\sigma_j}\right)=0. \tag{43}$$

Thus, the inequality (40) can be summarized as follows:

$$\dot{V}_2 \leq -k_0V_2+\varepsilon+w_3\theta_5(\nu(t)N(\xi)+1)\dot{\xi} \tag{44}$$

where k_0, ε are defined in theorem 1. Furthermore, we multiply e^{k_0t} to both sides of $\dot{V}_2$ and obtain

$$\frac{d\left(V_2e^{k_0t}\right)}{dt}\leq\left[\varepsilon+w_3\theta_5(\nu N(\xi)+1)\dot{\xi}\right]e^{k_0t}. \tag{45}$$

Moreover, integrating (45) from 0 to t yields

$$V_2(t)\leq w_3\theta_5e^{-k_0t}\int_0^t\left[(\nu(s)N(\xi)+1)\dot{\xi}(s)\right]e^{k_0s}ds + V_2(0)+\frac{\varepsilon}{k_0} \tag{46}$$

where $w_3\theta_5, V_2(0), \varepsilon/k_0$ are the bounded constants, and $\nu(t)$ is the bounded time-varying function. According to Lemma 2 in [32] or further results in [33], it can be concluded that $\xi(t)$, $V_2(t)$ and $e^{-k_0t}\int_0^t[(\nu(s)N(\xi)+1)\dot{\xi}(s)]e^{k_0s}ds$ are bounded. Inspired by [20], denote a constant ϖ_1 as the upper bound of $e^{-k_0t}\int_0^t[(\nu(s)N(\xi)+1)\dot{\xi}(s)]e^{k_0s}ds$, and let bound $\varpi = w_3\theta_{5\max}\varpi_1$. Thus, combining (46) and ϖ, the inequality (38) in Theorem 1 is obtained. The global boundedness of error z_2, z_3 is obtained immediately, and z_1 is also bounded. System state x, measurement error e and control input u are bounded since the estimation parameter $\hat{\theta}$, the desired trajectory y_d and its first 3-rd derivatives are all bounded.

In order to prove the asymptotic convergence, we give a Lyapunov function as

$$V_{2\theta}=V_2+\frac{1}{2}\tilde{\theta}^T\Gamma^{-1}\tilde{\theta}. \tag{47}$$

By virtue of ($P2$) in (10), (16), and (26), differentiate (47) as

$$\dot{V}_{2\theta}\leq w_3\theta_5e^{-k_0t}\int_0^t\left[(\nu(s)N(\xi)+1)\dot{\xi}(s)\right]e^{k_0s}ds - w_2k_2z_2^2-w_3k_3z_3^2. \tag{48}$$

Borrowing from [31], it can be deduced that the errors $z_2, z_3 \in L_2$ due to the boundedness of closed-loop signals. Hence, $\dot{z}_2, \dot{z}_3 \in L_\infty$. Using Barbalat's lemma obtains $z_2(t)\to 0$ as $t\to\infty$, and then the tracking error $z_1(t)\to 0$ as $t\to\infty$.

We now show that there exists a constant $T>0$, in which any interexecution interval is lower bounded by T. Denote $t_j^*=t_{j+1}-t_j$ as the interexecution internal.

Assuming $t_j^{*-}\to 0$, one obtains

$$\begin{aligned}&\lim_{t_j^{*-}\to 0}\left|e\left(t_j+t_j^{*-}\right)\right|\\&=\lim_{t_j^{*-}\to 0}\left|\mu\left(t_j+t_j^{*-}\right)-\mu\left(t_j^{*-}\right)\right|\\&\leq\lim_{t_j^{*-}\to 0}\left|-N\left(\xi(t_j+t_j^{*-})\right)\alpha_{3a}\left(t_j+t_j^{*-}\right)+N\left(\xi(t_j)\right)\alpha_{3a}(t_j)\right|\\&\quad+\lim_{t_j^{*-}\to 0}\left|(1+\sigma_j)\alpha_{3s}\left(t_j+t_j^{*-}\right)-(1+\sigma_j)\alpha_{3s}(t_j)\right|\\&\quad+\lim_{t_j^{*-}\to 0}\left|\text{sign}\left(z_3(t_j+t_j^{*-})\right)m_j-\text{sign}\left(z_3(t_j)\right)m_j\right|.\end{aligned} \tag{49}$$

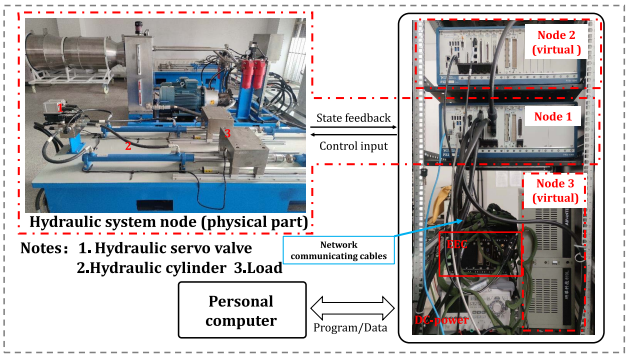

Fig. 3. Test-rig of the aero-engine HIL platform.

Using the continuous functions $N(\xi)$, α_{3a}, and α_{3s} to (49) has

$$\begin{aligned}&\lim_{t_j^{*-}\to 0}\left|e\left(t_j+t_j^{*-}\right)\right|\\&\leq\lim_{t_j^{*-}\to 0}\left|\text{sign}\left(z_3(t_j+t_j^{*-})\right)m_j-\text{sign}\left(z_3(t_j)\right)m_j\right|.\end{aligned} \tag{50}$$

For the rest proof, we adopt the same line with the analysis from [11]. The proof is divided into two parts. (i) When $z_3(t_j)\neq 0$, $\text{sign}(z_3(t_j))$ is a continuous function, (50) ensures the equality $\lim_{t_j^{*-}\to 0}|e(t_j+t_j^{*-})|=0$. (ii) When $z_3(t_j)=0$, the function $\text{sign}(z_3(t_j))$ is discontinuous, one has $\lim_{t_j^{*-}\to 0}|e(t_j+t_j^{*-})|\leq m_j$ based on (50). By the adaptive threshold triggered mechanism (33), the measurement error $e(t_{j+1})$ satisfies the following inequality:

$$\left|e\left(t_{j+1}\right)\right|=\left|e\left(t_j+t_j^*\right)\right|>\sigma_j\left|\mu\left(t_j\right)\right|+m_j\geq m_j. \tag{51}$$

The above analysis implies that the facts in case (i) and case (ii) are contradicted to the adaptive threshold triggering mechanism (51). Thus, the hypothesis is not true and then $t_j^{*-}>0$ holds for any interexecution internal. That is, there is a constant $T>0$ such that $t_j^*\geq T=\min\{t_1^{*-},t_2^{*-},\ldots,\}>0$. Note that if the asymptotic result is achieved, i.e., $z_3(t_j)=0$, the Zeno behavior can be excluded by virtue of case (ii). Moreover, in this context, the avoidance of Zeno behavior can also adopt the same line used in [19]. Namely, the Zeno behavior is eliminated. ■

Remark 3: Theorem 1 implies that the tracking error exponentially converges to an adjustable neighborhood of the origin by virtue of the proposed controller with or without parameter estimators. On the contrary, if there no system nonlinearities and the parametric uncertainties are resolved by adaptive laws, the closed-loop system achieves what the well-known adaptive controller performs, i.e., the asymptotic output tracking [2].

IV. Comparative Experiment

The aero-engine HIL distributed experiment platform with electro-hydraulic actuators is built for comparative experiments. The cable applies the RS-422 full-duplex communication protocol with bus topology shown in Fig. 3. The band rate is set as 614400bps, and three nodes are connected by cables, containing a physical node and two virtual nodes.

The physical node 1 denotes the hydraulic-driven device of the aero-engine HIL platform, including the electro-hydraulic system and data acquisition unit. Two virtual nodes represent other data-driven models with respect to some physical systems of the aero-engine HIL platform. In the physical node 1, the data acquisition device adopts PXI-8840 industrial computer, which performs the A/D and D/A transformation. The control voltage value of servo-valves is transmitted via the network cables and updated in accordance with (33). The state measurements are periodically transferred to the networked controller (EEC) using the same cables. Then we describe the physical part of node 1 as below. ATOS-DLHZO series proportional valve is used as the servo-valve and NADO-TPM series sensors are utilized to measure the position and velocity. The single-rod hydraulic cylinder is adopted with the piston diameter 40 mm and the rod diameter 25 mm. The maximum stroke and velocity are 0.5 m and 0.3 m/s, respectively. The supply pressure $P_s = 4$ Mpa and the payload is mass load with $M = 70$ kg. The proposed control scheme is tested and compared from the respective of tracking precision and the amount of data sent. To show the advanced performance, two types of comparative experiments are done.

Experiment 1 is used to show the advantages and flexibility of the adaptive threshold triggered mechanism, by contrast to the static mechanism in [11]. Then the experiment 2 analyzes and compares the networked control system performance with the limited communication resource for the proposed event-triggered control scheme and the traditional time-triggered adaptive robust motion controller [2].

A. Experiment 1: Comparison of the Different Event-Triggered Mechanisms

In a congested network environment, the traditional static event-based control schemes may be conservative in reducing bandwidth occupation. The adaptive event trigger proposed in this article can solve this issue, and the amount of data sent is actively increasing in the relaxed network environment.

To compare the difference of the proposed adaptive threshold triggered mechanism (33) and static threshold triggered mechanism in [11], two event-based control strategies are selected as follows.

C1: The adaptive threshold triggered mechanism (33) with $\sigma = 0, N(\xi) = -1$.

C2: The so-called fixed threshold triggered mechanism in [11] with static threshold parameters.

This test adopts S-curve trajectory, and the maximum velocity is 0.15 m/s and the maximum acceleration is 0.15 m/s^2, as shown in Fig. 4. The upper bounds on the feedback gains should be finite and determined by available bandwidth of the controller, which are often subject to the dynamics of servo-valve. A more pragmatic approach is thus to let $\alpha_{2s} = \alpha_{2s1} + \alpha_{2s2} = -K_2 z_2/\theta_{1\min}, \alpha_{3s} = \alpha_{3s1} + \alpha_{3s2} = -K_3 z_3/(g\theta_{5\min})$. It suggests that the nonlinear gains are replaced by the large enough linear gains such that $k_1 = K_2 = K_3 = 50$. Besides, other parameters are given by $w_2 = 10^8, w_3 = 1, \Gamma = \text{diag}\{10^{-11}, 0.01, 0.01, 10^{-8}, 10^{-7}, 0.001, 0.001\}, \hat{\theta}^T(0) = [0.0146, 0.72, 1.4, 0, 10^9, 0, 0]$. All the uncertain parameter boundaries were identified using the least squares estimation technique: $\theta^T_{\max} = [0.02, 4, 2, 4, 2 \times 10^9, 120, 120]$, $\theta^T_{\min} = [0.01, 0.3, 0.1, -4, 7 \times 10^8, -120, -120]$. Since most of operating conditions have been considered in the system identification, the obtained boundaries are effective and reliable for the motion control [22].

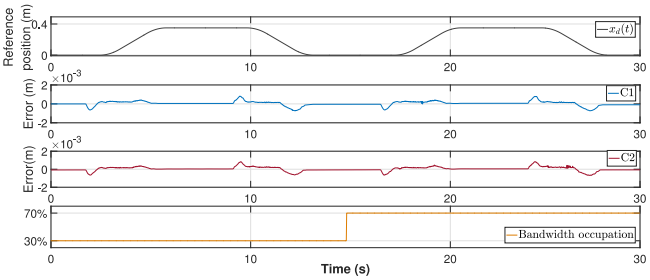

Fig. 4. Tracking performance comparison of two strategies in experiment 1.

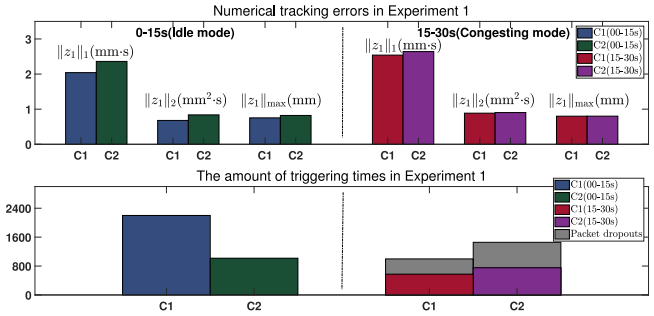

Fig. 5. Detailed numerical comparison of tracking error in experiment 1.

First, for a clear comparison, the network bandwidth is assumed to be idle at $t \in [0, 15)$, and congesting at $t \in [15, 30)$, where packets dropout according to the bandwidth occupation will happen in the congesting mode. The tracking error curves of C1 and C2 are compared in Fig. 4, and more detailed numerical comparison versions are shown in Fig. 5, where $\|z_1\|_1 = \int_{t_0}^{t_f} |z_1| dt$, $\|z_1\|_2 = \int_{t_0}^{t_f} |z_1|^2 dt$, and $\|z_1\|_{\max}$ represents the maximum value of $|z_1|$. In the congesting mode, i.e., $t \in [15, 30)$, C1 generates less amount of triggered times than C2 by noting Fig. 5. Intuitively, C1 can save the communication resource and reduce the burden of network bandwidth. Furthermore, the relaxed network environment greatly reduces the possibility of packet dropouts occurring in the process of data transmission, as displayed in Fig. 5. In the mode of congesting communications, C1 assures better tracking precision than C2 by virtue of the adaptive technique and the Nussbaum-type function. When the bandwidth turns to be idle in Fig. 5 (0-15s), more high-accuracy tracking is achieved by C1 with smaller thresholds compared to C2.

The comparative experiment results verify the flexibility of the proposed event-triggered mechanism. Especially, in the congesting bandwidth mode, the designed event trigger (33) reduces the amount of triggering times with larger thresholds, which further relaxes the network congestion. Meanwhile, the output tracking performance is efficiently enhanced for the idle case, which also helps raise the network bandwidth utilization.

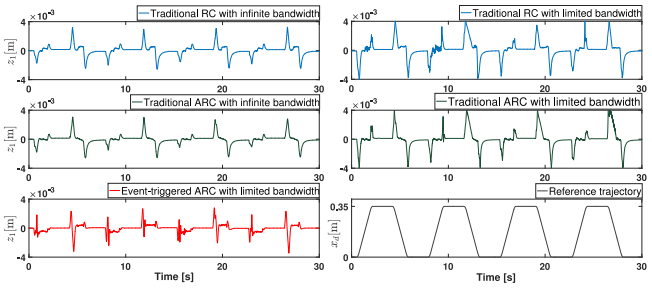

Fig. 6. Comparative tracking errors in experiment 2.

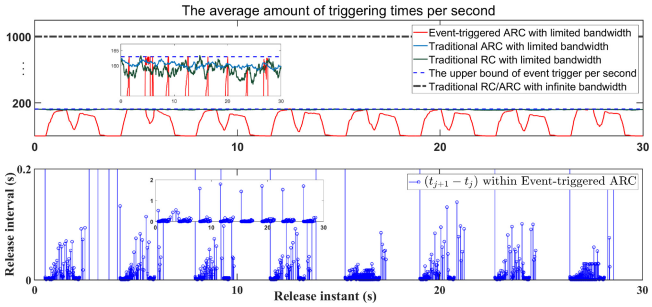

Fig. 7. Comparison of updating frequency in experiment 2.

TABLE I
NUMERICAL COMPARISON OF TRACKING ERRORS IN EXPERIMENT 2

	Controller	$\|z_1\|_1$ (mm·s)	$\|z_1\|_2$ (mm·s)	$\|z_1\|_{\max}$ (mm)
Infinite bandwidth	Traditional RC	12.92	15.16	3.21
	Traditional ARC	8.12	6.88	3.08
Limited bandwidth	Traditional RC	19.27	29.73	4.27
	Traditional ARC	16.34	26.52	4.03
	Event-triggered ARC	11.03	16.73	3.51

B. Experiment 2: Comparison of Motion Performance Under the Limited Bandwidth

It's proved that (33) has more advantages in the congesting communicating mode by contrast to the static mechanism. This experiment considers the bulk of the bandwidth hogged by two virtual nodes in the cable, as in Fig. 3. That is to say, the limited network resources are remained for updating control signals of node 1. Therefore, the presented event-triggered ARC control scheme is compared to the traditional ARC and RC (ARC without adaptive estimation) approaches [2] with the limited input updating frequency. If the updating frequency shown in Fig. 7 exceeds a set value, the data sent is supposed to drop out. For a clearer illustration, the new reference trajectory is employed with the maximum velocity 0.25 m/s and the maximum acceleration 1 m/s^2, as in Fig. 6.

The threshold parameters of event-triggered mechanism (33) are selected as $\sigma = 0.02, m = 0.02$, and $\xi(0) = 1.86$. The control gains are $k_1 = K_2 = K_3 = 60$ and adaptive tunable gains adopt the similar values as the experiment 1. The same control gains and/or adaptive gains are configurated for three motion control approaches.

Fig. 6 shows the tracking performance comparisons for three methods, and the numerical comparisons of tracking error are collected in Table I. It is evident to show that the adaptive technique helps improve the transient response and tracking precision by comparing ARC and RC approaches. Meanwhile, the comparisons between event-triggered ARC and ARC can demonstrate the necessity and significance of the event-based control in terms of the motion performance and the usage of network resources. Furthermore, the best tracking precision can be provided by the traditional ARC with infinite network resources. However, it is impractical to consider infinite communication resources for every node. We deploy a constraint of input updating frequency shown in Fig. 7, and the average number of triggering times per second for three controllers are also shown in this figure. Under this limitation, the traditional ARC and RC lose a large amount of input data, stochastically. Furthermore, the event-based ARC control scheme rejects and eliminates the effect of the measurement errors (arising from unsent data packets) with the aid of the Nussbaum-type function. As shown in Table I, in the presence of the bandwidth constraint, better tracking performance can be ensured by the proposed event-based ARC scheme, compared with traditional ARC and RC methods. In the end, the signals $\xi(t), N(\xi), z_3$ and parameter estimates are depicted in Figs. 9 and 10, respectively.

In conclusion, the experiment results suggest that the proposed algorithm is effective and practical. The event-triggered ARC presented in this article occupies less network resources than the time-triggered ARC used in [2], and also achieves high motion performance in the HIL networked platform.

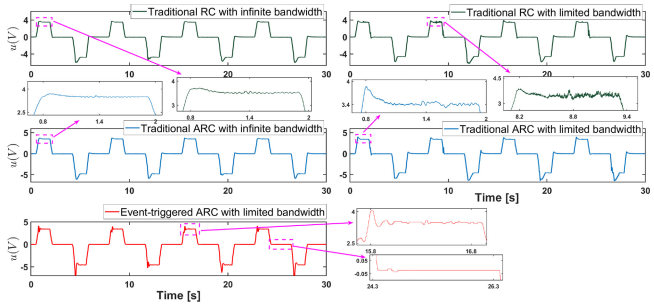

Fig. 8. Comparison of control inputs in experiment 2.

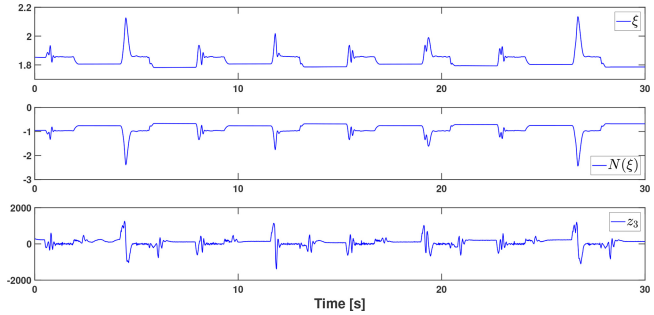

Fig. 9. Resulting signals of event-triggered ARC in experiment 2.

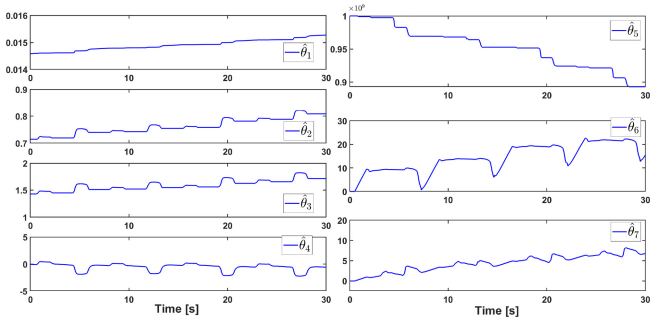

Fig. 10. Parameter estimates in experiment 2.

V. Conclusion

This article proposes an adjustable threshold triggered mechanism and synthesizes the event-based ARC motion control algorithm for hydraulic actuators to ensure as high as possible motion performance with the limited network bandwidth. The newly developed threshold triggered mechanism actively reduces the transmission times to a range accepted by the network transmission channel, and also helps relax the congested network environment. Meanwhile, the utilization rate of idle network resources can be raised by increasing the transmission times and thus improving the tracking precision. It's strictly proved that all the closed-loop hydraulic system signals are globally bounded, and the hydraulic system output achieves asymptotic tracking to the desired trajectory with the aid of the adaptive technique, the Nussbaum-type and sign functions. Besides, the Zeno behavior is avoided, successfully. Finally, comprehensive experiments have been done to reveal the benefits of the proposed algorithm which simultaneously satisfies the high motion performance and the constraint of the limited network bandwidth.

In experiment, the adaptive gain is hard to be selected for satisfactory estimation performance. It is thus suggested to study the dynamic-gain-based algorithm for simple implementation of ARC. In addition, future research can focus on the theoretical analysis between the control performance and the consumption of communication resources. These studies will be helpful for improving the current theory and application.

References

[1] H. E. Merritt, *Hydraulic Control Systems*. New York, NY, USA: Wiley, 1967.

[2] B. Yao, F. Bu, J. Reedy, and G.-C. Chiu, "Adaptive robust motion control of single-rod hydraulic actuators: Theory and experiments," *IEEE/ASME Trans. Mechatronics*, vol. 5, no. 1, pp. 79–91, Mar. 2000.

[3] R. M. Hessabi, A. Ashasi-Sorkhabi, and O. Mercan, "A new tracking error-based adaptive controller for servo-hydraulic actuator control," *J. of Vib. Control*, vol. 22, no. 12, pp. 2824–2840, Jul. 2016.

[4] B. Helian, P. Mustalahti, J. Mattila, Z. Chen, and B. Yao, "Adaptive robust pressure control of variable displacement axial piston pumps with a modified reduced-order dynamic model," *Mechatronics*, vol. 87, Nov. 2022, Art. no. 102879.

[5] S. Jaiswal, L. Pyrhönen, and A. Mikkola, "Computationally efficient coupling of Multibody dynamics and hydraulic actuators in simulating hydraulic machinery," *IEEE/ASME Trans. Mechatronics*, vol. 28, no. 3, pp. 1291–1302, Jun. 2023.

[6] A. Alleyne and R. Liu, "A simplified approach to force control for electro-hydraulic systems," *Control Eng. Pract.*, vol. 8, no. 12, pp. 1347–1356, Dec. 2000.

[7] J. Pedro and O. Dahunsi, "Neural network based feedback linearization control of a servo-hydraulic vehicle suspension system," *Int. J. of Appl. Math. Comput. Sci.*, vol. 21, no. 1, pp. 137–147, Mar. 2011.

[8] D. Won, W. Kim, and M. Tomizuka, "Nonlinear control with high-gain extended state observer for position tracking of electro-hydraulic systems," *IEEE/ASME Trans. Mechatronics*, vol. 25, no. 6, pp. 2610–2621, Dec. 2020.

[9] P. Tabuada, "Event-triggered real-time scheduling of stabilizing control tasks," *IEEE Trans. Autom. Control*, vol. 52, no. 9, pp. 1680–1685, Sep. 2007.

[10] W. Wang, C. Wen, J. Huang, and J. Zhou, "Adaptive consensus of uncertain nonlinear systems with event triggered communication and intermittent actuator faults," *Automatica*, vol. 111, Jan. 2020, Art. no. 108667.

[11] C.-H. Zhang and G.-H. Yang, "Event-triggered global finite-time control for a class of uncertain nonlinear systems," *IEEE Trans. Autom. Control*, vol. 65, no. 3, pp. 1340–1347, Mar. 2019.

[12] H. Chen, G. Zong, X. Zhao, F. Gao, and K. Shi, "Secure filter design of fuzzy switched CPSs with mismatched modes and application: A multidomain event-triggered strategy," *IEEE Trans. Ind. Informat.*, vol. 19, no. 10, pp. 10034–10044, Oct. 2023.

[13] J. Chen, L. Lyu, Z. Fei, W. Xia, and X.-M. Sun, "Event-triggered adaptive robust control for a class of uncertain nonlinear systems with application to Mechatronic system," *IEEE Trans. Ind. Informat.*, vol. 19, no. 12, pp. 11800–11808, Dec. 2023.

[14] Z. Fei, W. Chen, and X. Zhao, "Interval estimation for asynchronously switched positive systems," *Automatica*, vol. 143, Sep. 2022, Art. no. 110427.

[15] K. Zhang, R. Su, H. Zhang, and Y. Tian, "Adaptive resilient event-triggered control design of autonomous vehicles with an iterative single critic learning framework," *IEEE Trans. Neural Netw. Learn. Syst.*, vol. 32, no. 12, pp. 5502–5511, Dec. 2021.

[16] V. Djordjevic, H. Tao, X. Song, S. He, W. Gao, and V. Stojanović, "Data-driven control of hydraulic servo actuator: An event-triggered adaptive dynamic programming approach," *Math. Biosciences Eng.: MBE*, vol. 20, no. 5, SI, pp. 8561–8582, Apr. 2023.

[17] H. Chen, G. Zong, F. Gao, and Y. Shi, "Probabilistic event-triggered policy for extended dissipative finite-time control of MJSs under Cyber-attacks and actuator failures," *IEEE Trans. Autom. Control*, vol. 68, no. 12, pp. 7803–7810, Dec. 2023.

[18] Z. Fei, X. Wang, M. Liu, and J. Yu, "Reliable control for vehicle active suspension systems under event-triggered scheme with frequency range limitation," *IEEE Trans. Syst., Man, Cybern.: Syst.*, vol. 51, no. 3, pp. 1630–1641, Mar. 2021.

[19] L. Xing, C. Wen, Z. Liu, H. Su, and J. Cai, "Event-triggered adaptive control for a class of uncertain nonlinear systems," *IEEE Trans. Autom. Control*, vol. 62, no. 4, pp. 2071–2076, Apr. 2016.

[20] H. Pan, X. Chang, and D. Zhang, "Event-triggered adaptive control for uncertain constrained nonlinear systems with its application," *IEEE Trans. Ind. Informat.*, vol. 16, no. 6, pp. 3818–3827, Jun. 2019.

[21] X. Yuan, B. Chen, and C. Lin, "Neural adaptive fixed-time control for nonlinear systems with full-state constraints," *IEEE Trans. Cybern.*, vol. 53, no. 5, pp. 3048–3059, May 2023.

[22] L. Lyu, Z. Chen, and B. Yao, "Advanced valves and pump coordinated hydraulic control design to simultaneously achieve high accuracy and high efficiency," *IEEE Trans. Control Syst. Technol.*, vol. 29, no. 1, pp. 236–248, Jan. 2021.

[23] Z. Chen, S. Zhou, C. Shen, L. Lyu, J. Zhang, and B. Yao, "Observer-based adaptive robust precision motion control of a multi-joint hydraulic manipulator," *IEEE/CAA J. of Automatica Sinica*, vol. 11, no. 5, pp. 1213–1226, May 2024.

[24] J. Huang, W. Wang, C. Wen, and G. Li, "Adaptive event-triggered control of nonlinear systems with controller and parameter estimator triggering," *IEEE Trans. Autom. Control*, vol. 65, no. 1, pp. 318–324, Jan. 2020.

[25] D. Yang, G. Zong, Y. Shi, and P. Shi, "Model reference adaptive tracking control of uncertain Markovian hybrid switching systems," *SIAM J. Control Optim*, vol. 61, no. 2, pp. 434–457, 2023.

[26] W. Shi, M. Hou, and G. Duan, "A preset-trajectory-based singularity-free preassigned performance control approach," *IEEE Trans. Autom. Control*, vol. 69, no. 9, pp. 6183–6190, Jan. 2025.

[27] H. Gao, Y. Liu, W. Sun, and X. Yu, "Adaptive wavelet tracking control of dual-linear-motor-driven gantry stage with suppression of crossbeam rotation," *IEEE/ASME Trans. Mechatronics*, vol. 29, no. 1, pp. 97–105, Feb. 2024.

[28] Z.-J. Yang, Y. Fukushima, and P. Qin, "Decentralized adaptive robust control of robot manipulators using disturbance observers," *IEEE Trans. Control Syst. Technol.*, vol. 20, no. 5, pp. 1357–1365, Sep. 2012.

[29] W. Sun, H. Gao, and B. Yao, "Adaptive robust vibration control of full-car active suspensions with Electrohydraulic actuators," *IEEE Trans. Control Syst. Technol.*, vol. 21, no. 6, pp. 2417–2422, Nov. 2013.
[30] Z.-G. Wu, Y. Xu, R. Lu, Y. Wu, and T. Huang, "Event-triggered control for consensus of Multiagent systems with fixed/switching topologies," *IEEE Trans. Syst., Man, Cybern.: Syst.*, vol. 48, no. 10, pp. 1736–1746, Oct. 2018.
[31] Y. Xudong and J. Jingping, "Adaptive nonlinear design without a priori knowledge of control directions," *IEEE Trans. Autom. Control*, vol. 43, no. 11, pp. 1617–1621, Nov. 1998.
[32] S. S. Ge and J. Wang, "Robust adaptive tracking for time-varying uncertain nonlinear systems with unknown control coefficients," *IEEE Trans. Autom. Control*, vol. 48, no. 8, pp. 1463–1469, Aug. 2003.
[33] H. E. Psillakis, "Further results on the use of Nussbaum gains in adaptive neural network control," *IEEE Trans. Autom. Control*, vol. 55, no. 12, pp. 2841–2846, Dec. 2010.

Jixiang Chen received the B.E. degree in marine engineering from Dalian Maritime University, Dalian, China, in 2018, and the M.E. degree in control engineering and the Ph.D. degree in control theory and control engineering from Dalian University of Technology, Dalian, in 2020 and 2024, respectively.

Since 2024, he has been with the College of Marine Electrical Engineering, Dalian Maritime University, where he is currently a Lecturer. His research interests include synchronization control, adaptive control, finite-time control, and electromechanical systems.

Zhongyang Fei (Senior Member, IEEE) received the B.E. and M.S. degrees in control science and engineering from Harbin Institute of Technology, Harbin, China, in 2007 and 2009, respectively, and the Ph.D. degree in mechanical engineering from Mechanical Engineering and Materials Science Department, Washington University in St. Louis, St. Louis, MO, USA, in 2013.

He is currently a Professor with the Key Laboratory of Intelligent Control and Optimization for Industrial Equipment of Ministry of Education, and also with School of Control Science and Engineering, Dalian University of Technology.

Litong Lyu received the B.E. and Ph.D. degrees in mechatronics engineering from Zhejiang University, Hangzhou, Zhejiang, China, in 2015 and 2020, respectively.

Since 2020, he has been with the School of Mechanical Engineering, Shijiazhuang Tiedao University, Hebei, China, where he is currently an Associate Professor.

Weiguo Xia received the B.Sc. and M.Sc. degrees in applied mathematics from Southeast University, Nanjing, China, in 2006 and 2009, respectively, and the Ph.D. degree in systems and control from the Faculty of Mathematics and Natural Sciences, ENTEG, University of Groningen, Groningen, The Netherlands, in 2013.

He is currently a Professor with the School of Control Science and Engineering, Dalian University of Technology, Dalian, China. From 2013 to 2015, he was a Postdoctoral Researcher with the ACCESS Linnaeus Centre, Royal Institute of Technology, Stockholm, Sweden.

Prof. Xia is an Associate Editor for SYSTEMS & CONTROL LETTERS.

Xi-Ming Sun (Senior Member, IEEE) received the Ph.D. degree in control theory and control engineering from the Northeastern University, Shenyang, China, in 2006.

From August 2006 to December 2008, he worked as a Research Fellow with the Faculty of Advanced Technology, University of Glamorgan, Pontypridd, U.K. He then visited the School of Electrical & Electronic Engineering, Melbourne University, Melbourne, VIC, Australia, in 2009, and the Polytechnic Institute of New York University, Brooklyn, NY, USA, in 2011, respectively. He is currently a Professor with the School of Control Science and Engineering, Dalian University of Technology, Dalian, China.

Prof. Sun was awarded the Most Cited Article 2006–2010 from the Journal of *Automatica* in 2011. He serves as Associate Editor of IEEE TRANSACTIONS ON CYBERNETICS.